Journal of Materials Chemistry A

Accepted Manuscript

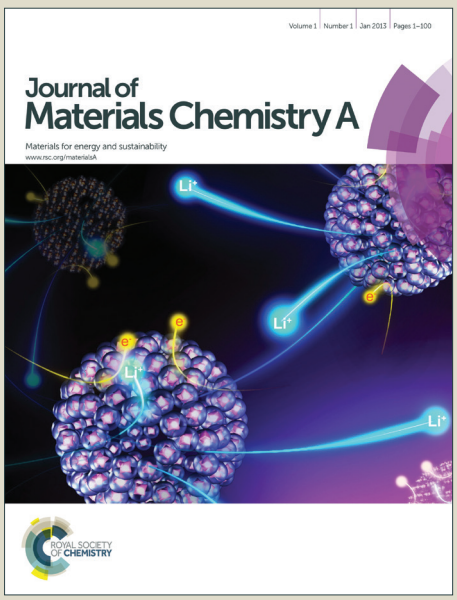

ROYAL SOCIETY OF CHEMISTRY

www.rsc.org/materialsA

Journal Name

RSCPublishing

ARTICLE

ZnO Nanorod/nanoparticle Hierarchically Structure Synthetized through a Facile In-situ Method for Dye-sensitized Solar Cells

Cite this: DOI: 10.1039/xoxxoooooox

Received ooth January 2012,
Accepted ooth January 2012

DOI: 10.1039/xoxxoooooox

www.rsc.org/

Rui Gao[a], Yixiu Cui[a], Xiaojiang Liu[a], Liduo Wang*[b], Guozhong Cao*[c,d]

A novel ZnO nanorod/nanoparticle (NR/NP) hierarchically structure on zinc foil has been fabricated through a chemical bath deposition method. When used as flexible photoanode for DSSCs, such structure demonstrated enhanced dye-loading and electron life time as compared to NR structure. It also retarded the charge recombination and kept the electron diffusion length of NR structure meanwhile. As a result, the power conversion efficiency of the DSSCs based on NR/NP structure increased from 1.35% to 3.63% with 169 % enhancement as compared to that based on ZnO NR.

1. Introduction

Since the breakthrough in power conversion efficiency reported in 1991[1], dye-sensitized solar cells (DSSCs) have been considered as an alternative to the conventional silicon based solar cells due to its lower cost and easier fabrication as well as less sensitive to the incident angel and intensity of light. By 2011, a high power conversion efficiency of 12.3% was achieved[2], which is close to the efficiency of commercial silicon solar cells. Much attention have been focused on efficiency enhancement and stability improvement of DSSCs[3]. Besides TiO_2, ZnO has been widely intensively studied as photoanode for DSSCs in recent years[4] as its easier synthesis and higher electron mobility[5]. A high conversion efficiency of 7.5% had been obtained in 2011[6]. Furthermore, conversion efficiency of ZnO DSSCs based on quasi-solid electrolyte also reached high conversion efficiency[7-9], which is up to 6.46%[10].

Flexible DSSCs have been attracting significant interest because of its lightweight, low cost roll-to-roll production and potential applications in powering mobile electronic products. Up to now, two kinds of flexible substrates have been used, metal sheets[11] and polymer substrates[12]. Compared to polymer substrate, metal sheets have low resistance, and easier to make flexible DSSCs devices.[11, 13] However, DSSCs device based on metal sheets obtained much lower conversion efficiency than that based on FTO glass.[14, 15] As a result, much study has been done to enhance the efficiency of such kind of DSSCs[16, 17].

As its high electron mobility, ZnO with ordered structures, especially one-dimensional nanostructures were considered as ideal structure for photoanode[18-21]. ZnO nanotubes, nanorods, and nanorods have been synthesized and expected to obtain highly conversion efficiency of DSSCs. However, the 1-D structures have a much smaller surface area for dye adsorption compared with nanoparticles, which causing a lower photocurrent and efficiency. Constructing hierarchical morphologies based on 1-D structures and nanoparticles turns out to be an effective way to improve the surface area significantly[22]. Cao et al made nanoparticles and nanorod array hybrid photoanode and obtained 4.24% conversion efficiency[23]. Recently, a nanorod-nanopartilces hierarchical structure of ZnO has been used in DSSCs, which obtained a high conversion efficiency of 7.14%[24]. However, the synthesizing method used now needed high temperature[25], which increased the power consumption and cost[26]. Direct precipitation process[27, 28] is an efficient way to synthesize ZnO with specific shapes at low temperature[29, 30]. Herein, we report an in-situ precipitation method[31] to synthesize nanoflowers composited of nanorods (NR) on the zinc foil which could be used as flexible photoanode for DSSCs[32]. Compared with other routes such as electrochemical deposition, physical/chemical vapor deposition or hydrothermal methods, this method features simpler operation and lower cost, and is more ideal for industrial production. To improve the performance of DSSCs based on such photoanode, a nanorod/nanoparticles (NRs/NPs) hierarchical structure has been fabricated with a chemical bath deposition (CBD) method in a $Zn(OAc)_2{\cdot}2H_2O$ methanolic solution. When ZnO NRs/NPs composite photoanode is fabricated, it combined high electron transport abilities and large dye absorption areas, increasing the conversion efficiency significantly of DSSCs based on flexible photoanode.

2. Experimental

The alkali zincate solution was prepared by dropping 20 mL 0.125 M aqueous solution of $Zn(NO_3)_2{\cdot}6H_2O$ into 20 mL 1.0 M aqueous solution of KOH under stirring. The growth of ZnO nanorods assembled nanosflowers were achieved by suspending a clean zinc foil (Alfa Asear, 99.9%, 0.25 mm thick) upside down in 40 mL zincate solution and sealing the system in a beaker. The zinc foil was feathered by sanding and then cleaned through ultrasonic vibration in pure ethanol before used. After reaction at 40 ^oC for 4 h, the zinc foil was taken out and rinsed with de-ionized water. The second process was transferring the zinc foil obtained in the last process into a 20 mL glass bottle containing 0.01 M $Zn(OAc)_2{\cdot}2H_2O$ methanolic solution, and heated at 40 ^oC for 12 h.

The ZnO photoanode was sintered at 350 ^oC, then sensitized in 0.3mM N719 absolute ethanol solution for 60 min, followed

by cleaning with absolute ethanol. The electrolyte is a liquid admixture containing 0.5 M tetrabutylammonium iodide, 0.1 M lithium iodide, 0.1 M iodine, and 0.5 M 4-tert-butylpyridine in acetonitrile. A transparent platinized conductive glass was used as the counter electrode, which is bought from Dyesol Ltd. directly. When assembling the back-illuminated DSSCs, the electrolyte was sandwiched by a sensitized ZnO on the zinc foil and a counter electrode with two clips. A 60 μm thick adhesive tape of was used to separate the photoanode and counter electrode. The illumination was from the direction of counter electrode.

The UV-Vis reflectance absorption spectra were measured with a Hitachi U-3010 spectroscope. The morphologies of the ZnO films were characterized by SEM (JSM 7401). Photocurrent-voltage (*I-V*), dark current measurements, monochromatic incident photon-to-electroncon versione fficiency (IPCE), electrochemical impedance spectroscopy (EIS) and Intensity modulated photovoltage/ photocurrent spectrum (IMVS/IMPS) were investigated by ZAHNER CIMPS electrochemical workstation.

3. Results and discussion

Different ZnO structures have been fabricated on zinc foil through a precipitation method at different temperature. Fig. 1 (a)(b) showed that as the reaction in a lower temperature (20 ^{o}C), the precipitation is difficult to occur, forming a disordered nanoparticles structure. As the reaction temperature increased to 40 ^{o}C, nanorods assembled nanoflowers (NFs) were obtained on the zinc foil, which were shown in Fig. 1 (c)(d). The size of NFs is about 1-1.5 μm. As the reaction temperature further increased to 60 ^{o}C, part of ZnO nanorods turned out to nanosheets. At the same time, the size of NF also increased to about 3 μm, seen in Fig. 1 (e)(f). The formation process of

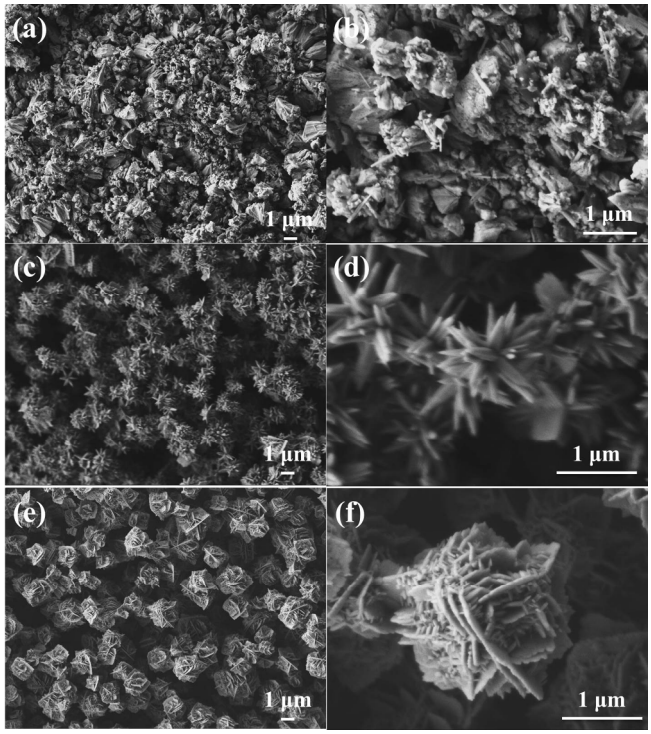

Fig.1 SEM images of different ZnO films on the zinc foil obtained by precipitation method at different temperature (a) (b) 20 ^{o}C, (c) (d) 40 ^{o}C (e) (f) 60 ^{o}C.

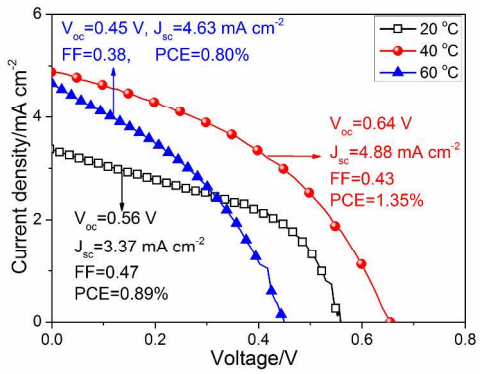

Fig.2 I-V curves under 100 mW cm^{-2} illumination of DSSCs based on ZnO obtained by precipitation method at different temperature.

hierarchically structures shown in Fig. 1 (c) and (e) is similar to that reported in Ref. 7.

We tested the photovoltaic performance of DSSCs based on different ZnO structured obtained at different reaction temperature which were shown in Fig. 1. As shown in Fig. 2, the device based on ZnO NR assembled nanoflowers synthesized at 40 ^{o}C showed the highest V_{oc}, J_{sc} and conversion efficiency, which was 1.35% under 100 mW cm^{-2} illumination. It could be explained that the NR assembled nanoflower combined the efficient dye-loading and good electron transport. When the reaction temperature is as low as 20 ^{o}C, the disordered ZnO nanoparticles has been formed. It could not adsorb dye molecules efficiently, thus the photocurrent is rather low. As the reaction time increased to 60 ^{o}C, the dye-loading of ZnO photoanode could become lower than that obtained at 40 ^{o}C as the nanosheets assembled nanoflowers is much larger than the NR assembled sample, which could cause the decrease of specific surface area. The verified V_{oc} and FF with the different morphologies of ZnO could be explained as followed. As the reaction temperature is 20 ^{o}C, we obtained a disordered structure, which has a poor electron transport in the ZnO film. Thus the charge recombination increased. Compared the sample obtained in 60 ^{o}C, the 40 ^{o}C sample has a smaller sized nanoflowers structure, which could cause a better connection between different nanoflowers. Furthermore, the 40 ^{o}C sample with 1-D structure has a better electron transport than the 2-D structure of 60 ^{o}C sample. As a result, the possibility of charge recombination is smaller than that of 60 ^{o}C sample. As a result, the V_{oc} , J_{sc} and FF all decreased compared to 40 ^{o}C sample.

The growth of ZnO on zinc foil could be presented as following reactions[31]

$$Zn + 2H_2O + 2OH^- \rightarrow Zn(OH)_4^{2-} + H_2 \quad (1)$$

$$Zn(OH)_4^{2-} \rightarrow ZnO + H_2O + 2OH^- \quad (2)$$

At first, the dissolution of Zn atoms into the solution caused a concentration gradient of zincate ion, and then NR arrays are

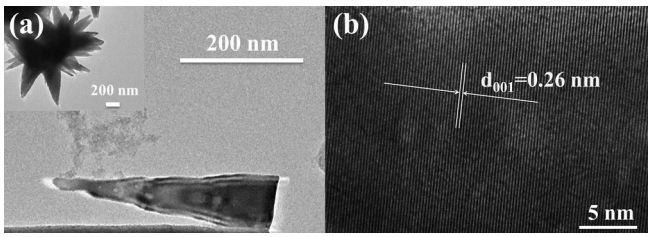

Fig. 3 HRTEM images of ZnO NR assembled nanoflowers on the zinc foil fabricated at 40 °C during the precipitation process in the alkaline solution.

formed on the zinc foil (see Fig. S1) during the precipitation reaction with a short time at 40 °C, which is same as reported in Ref. 28. When the precipitation process continued, more and more ZnO deposited on the zinc foil. The NR arrays could strengthen the connection of zinc foil and ZnO precipitated on it, which could benefit electron transfer from ZnO to the zinc foil.

As shown in Fig. 3, HRTEM image revealed that the NRs are a single crystal. According to the features of the diffraction pattern, the preferential growth direction of the ZnO NRs is their [001] direction. The displayed lattice spacing of 0.26 nm corresponds to the lattice spacing of the ZnO (002) plane, which also indicates that the [001] direction is the preferential growth direction[33]. During the process of ZnO nanocrystal growth, the dissolution of Zn atoms into the solution caused a concentration gradient of zincate ion from the bottom to the top of NRs. As a result, the growing rates along the ZnO (001) planes decreased from the nanocrystal roots to the tips and finally NRs shown in Fig. 1(c) (d) and Fig. 3 were formed. This could be explained that the excess OH^- anions retarded the growth of other facets. This result also accorded with that in Ref. 22. However, the effect of the concentration gradient was weakened by increasing the reaction temperature as it could cause much faster growth of ZnO nanocrystals. Thus as the reaction temperature increased to 60 °C, besides of [001], ZnO growth in [100] direction started to appear, formed a nanosheets composited nanoflowers shown in Fig. 1 (e)(f).

As shown in Fig. 2, the 40 °C sample obtained the highest efficiency of 1.35% during the three different samples. However, one key challenge of using such 1D nanostructure in DSSCs is their relatively lower specific surface area compared to nanoparticles, resulting in insufficient dye adsorption and, therefore, low light-harvesting efficiency. Hierarchical morphologies consisting of 1 D nanorods and 0 D nanoparticles would offer an effective way to synergistically combine the high specific surface area with easy and fast charge transfer. Thus we fabricate such a hierarchical structure of ZnO NR/NP through a chemical bath deposition method in $Zn(OAc)_2{\cdot}2H_2O$ methanolic solution.

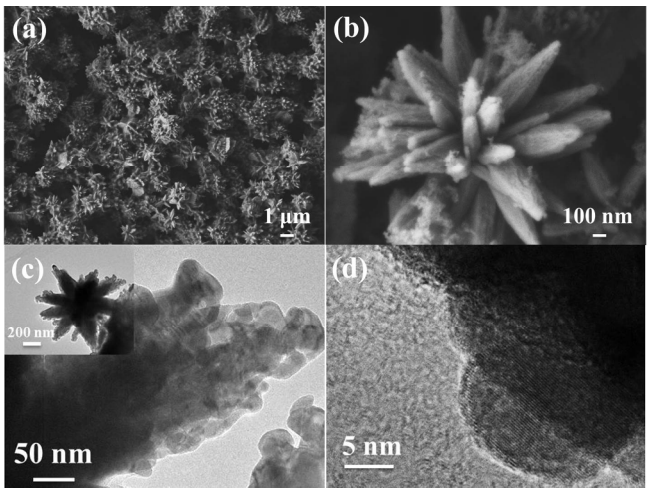

Fig. 4 (a) (b) SEM images of ZnO nanoflower composited of nanorod/nanoparticles. (c)(d) HRTEM images of ZnO nanorods/nanoparticles grown in 0.01 M $Zn(OAc)_2{\cdot}2H_2O$ methanolic solution heated at 40 °C for 12 h.

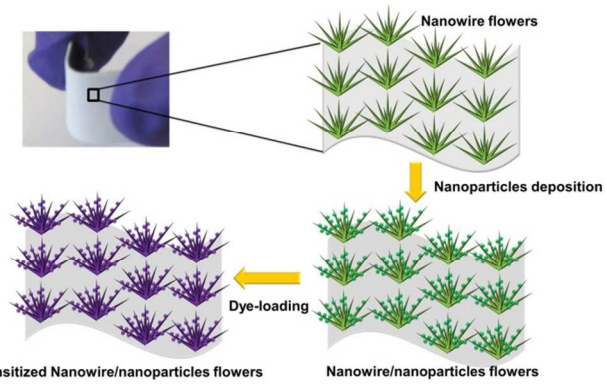

Scheme. 1 Schematical illustration of nanoparticles deposition on the nanorods and sensitizing processes.

As shown in Fig. 4 (a) and (b), after treated in $Zn(OAc)_2{\cdot}2H_2O$ methanolic solution, nanoparticles were formed and attached on the NRs. The surface of NRs became much rougher, which indicated that the surface area increased. As shown in Fig. 4 (c) and (d), the HRTEM images revealed nanoparticles attached on the NRs and the NPs were about 10 nm in diameter. The attachment process of NPs on the NRs and sensitization were illustrated in Scheme 1. The increased surface area enhanced amount of dye loaded. Table 1 compared the dye-loading amount in ZnO NRs with that in NRs/NPs and showed the increase from 89 to 162 nmol cm^{-2}, with an 86.2% relative enhancement. A large dye adsorption amount would capture more photons, resulting in a larger IPCE and J_{sc}, and thus improving the power conversion efficiency of DSSCs.

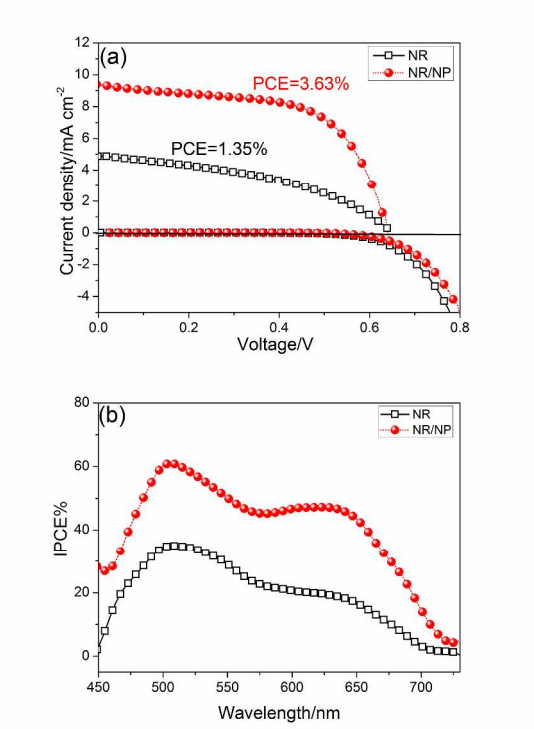

Fig. 5 (a) I-V curves (b) IPCE of DSSCs based on ZnO NR and NR/NP photoanode under 100 mW cm^{-2} illumination. The dark current curves were also added to (a).

Table 1 Photovoltaic parameters of DSSCs based on ZnO NR and NR/NP photoanodes.

Samples	J_{sc}/mA/cm^2	V_{oc}/V	FF%	PCE/%	Dye-loading/ nmol cm^{-2}
NRs	4.88	0.64	43.2	1.35	89
NRs/NPs	9.40	0.64	60.4	3.63	162

As shown in Fig. 5 (a) and Table 1 showed the photovoltaic performance of DSSCs based on ZnO NR and NR/NP photoanode. Compared to ZnO NR, the short-circuit current density (J_{sc}) of device based on NR/NP photoanode increase from 4.88 mA/cm^2 to 9.40 mA/cm^2, with a 92.6% increasing relatively. As discussed above, the increased photocurrent density is due to much larger dye-loading with NR/NP structure. Besides of increasing J_{sc}, the NR/NP structure also improved the FF of DSSCs compared with the device based on ZnO NR. As shown in Fig. 5 (a) and Table.1 the FF increased from 43.2% to 60.4% as the ZnO NR turned to NR/NP structure. At the same time, the V_{oc} did not change during the NP deposition process. As a result, compared to DSSCs based on ZnO NR, the convrsion efficiency of that based on NR/NP hierarchically structure increased from 1.35% to 3.63%, showing a significantly enhancement of 169%. This is also a high conversion efficiency of ZnO DSSCs based on flexible metal foil photoanode. The performance stability of DSSCs based on the flexible photoanode during bending is also well. As shown in Fig. S3, though the J_{sc} and Voc decrease a little after bending, the conversion efficiency almost maitained as same as before bending.

As shown in Fig. 5 (a), the dark current also decreased as the ZnO NR changed to NR/NP hierarchically structure, indicating a weaker back reaction in devices based on such photoanode.

As shown in Fig. 5 (b), compared to the DSSCs device based on ZnO NR photoanode, the IPCE of the DSSCs based on ZnO NR/NP photoanode increased significantly, which is about two times of the former. The enhancement of IPCE is considered to be caused by the increased dye-loading amount as the ZnO NR structure changed to NR/NP hierarchically structure, which is shown in Table. 1. Hence, such hierarchical ZnO photoanode would maximize the use of solar light, which enhance the light harvesting efficiency and J_{sc} of DSSCs.

To further investigate the electron transport and recombination properties in such two different structures, we tested EIS and IMVS/IMPS of DSSCs devices based on ZnO NR and NR/NP photoanodes. As shown in Fig. 6 (a), in the frequency range of 10^5-10^3 Hz, the impedance associated with the charge transfer process occurring at Pt electrode/electrolyte interface is determined, which is characterized by the charge transfer resistance (R_1) and the capacitance (CPE_1). In the middle frequency range of 10^3-10^0 Hz, the impedance related to the charge recombination process at the TiO_2/dye/electrolyte interface can be described by R_2 and the CPE_2. And in the low frequency 0.1-10 Hz, the Warburg diffusion impedance (Z_w) within the electrolyte will be estimated. The sheet resistance (R_s) of substrate, charge transfer resistance of the counter electrode (R_1) and charge transfer resistance (R_2) were analyzed by Z-view software using an equivalent circuit inset of Fig.6 (a).

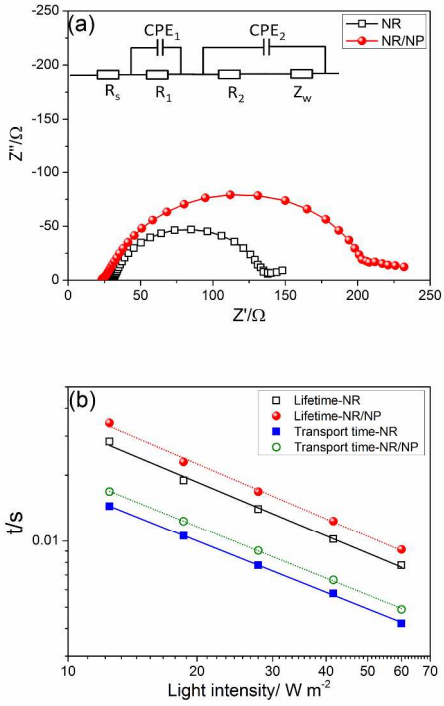

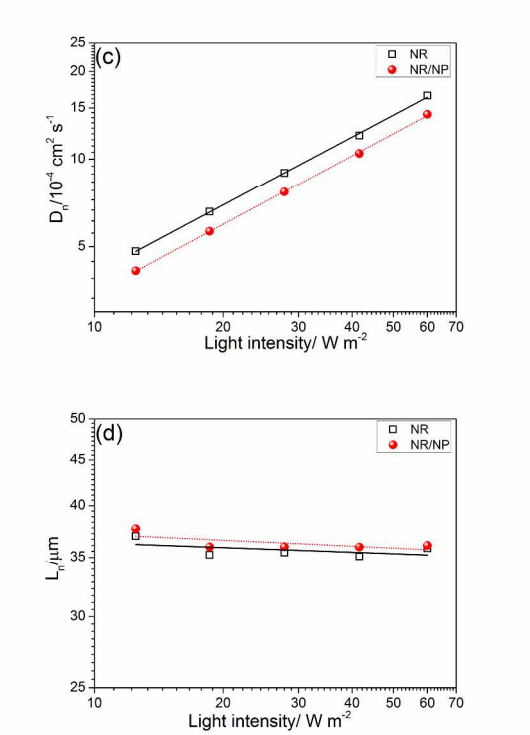

Fig. 6 (a) Nyquist plots under dark condition with -0.8 V bias voltage (b) Electron collection timeand lifetime obtained from IMPS and IMVS characterization respectively (c) electron diffusion coefficient D_n (d) electron diffusion length L_n as a function of light intensity for DSSCs based on ZnO NR and NR/NP photoanodes.

Z_w accounts for a finite length Warburg diffusion while CPE represents the constant phase element. As shown in Fig.6 (a) and Table.2, the cells based on ZnO NR and NR/NP processed similar R_s and R_1. Compared to cells based on ZnO NR, the charge recombination resistance of cell based on ZnO NR/NP increased from 105 Ω to 178 Ω, indicating more difficult for charge recombination. Thus the back reaction was decreased. The result also accorded with the results of dark current measurement decreasing shown in Fig.6 (b).

Table 2 The resistance fitted from the electrochemical impedance spectra of DSSCs based on ZnO NR and NR/NP photoanodes.

Samples	R_s/Ω	R_1/Ω	R_2/Ω
NR	28.4	5.6	105
NR/NP	23.2	6.3	178

The weakened charge recombination could be explained with two reasons. At first, the connection could be improved during the nanoparticles deposition process, which connecting several NFs together. As a result, the electron is easier to be collected by zinc foil substrate, decreasing the possibility of charge recombination. Besides, within the NP deposition, the surface defect states could be passivated, then decreasing the charge recombination.

Fig. 6 (b) showed the time constants of electron transport (τ_c) and electron lifetime (τ_r) as a function of light intensity, showing that all time constants decrease with increasing light intensity. The ZnO NR/NP anode showed longer electron lifetime than NR, which is due to its weaker charge recombination than NR anode. On the other hand, the transport time (obtained from IMPS measurement) of a ZnO NR/NP based cell is larger than that of a NR based cell which could be attributed to the presence of numerous boundaries between the ZnO nanorod and nanoparticcles branches according to the HRTEM results shown in Fig. 3. As the electron transport time of ZnO NR/NP is larger, its electron diffusion coefficient (D_n) is smaller than that of ZnO NR with calculated by equation $D_n = L^2/2.35\tau_c$, which was shown in Fig. 6(c)[34]. The results of IMVS and IMPS also could be explained by a dominant surface diffusion hypothesis.[35]

Electron diffusion length ($L_n=(D_n\tau_r)^{0.5}$) suggests whether the injected electron can transport to external circuit which influence the J_{sc} and PCE[36]. Fig. 6 (d) represented the L_n of DSSCs based on ZnO NR and NR/NP, which is both about 36 μm, almost without any differences, indicating L_n had maintained as changing NR to NR/NP structure. This result is better than that reported before. As a result, we fabricated our film with such thickness (about 38μm) to maximum the conversion efficiency of DSSCs (see Fig S2). The maintained L_n also ensure the NR/NP structure to increase the photocurrent and FF and keep the V_{oc}, thus enhance the conversion efficiency significantly.

4. Conclusions

A novel ZnO NR/NP hierarchically structured film on zinc foil has been fabricated through a facile chemical bath deposition method at low temperature. Such ZnO NR/NP hierarchically structured films demonstrated enhanced dye-loading and electron life time when used as photoanodes as compared to ZnO NR. It also retarded the charge recombination and kept the electron diffusion length of NRs. As a result, it increased the conversion efficiency of the DSSCs with a significant 169 % relative enhancement compared to that based on ZnO NR.

Acknowledgements

This work has been supported in part by the US Department of Energy, Office of Basic Energy Sciences, Division of Materials and Engineering under Award No. DE-FG02-07ER46467 (Q.F.Z.) on the microstructure characterization and some power conversion efficiency measurements, National Science Foundation (DMR-1035196), the National Natural Science Foundation of China under Grant No. 51273104 and the National Key Basic Research and Development Program of China under Grant No. 2009CB930602.

Notes and references

[a] R Gao, Y. X. Cui, X. J. Liu
Institute of Electronic Engineering,
China Academy of Engineering Physics,
Mianyang 621900, Sichuan, China.
[b] Prof. L. D. Wang
Key Lab of Organic Optoelectronics & Molecular Engineering of Ministry of Education, Department of Chemistry, Tsinghua University,
Beijing 100084, China
Email: chldwang@mail.tsinghua.edu.cn

[c] Prof. G. Z. Cao
Department of Materials Science and Engineering,
University of Washington,
Seattle, WA 98195, USA
Email: gzcao@u.washington.edu
[d] Prof. G. Z. Cao
Beijing Institute of Nanoenergy and Nanosystems,
Chinese Academy of Sciences,
Beijing 100085, China

† Footnotes should appear here. These might include comments relevant to but not central to the matter under discussion, limited experimental and spectral data, and crystallographic data.
Electronic Supplementary Information (ESI) available: [details of any supplementary information available should be included here]. See DOI: 10.1039/b000000x/

1. B. Oregan and M. Gratzel, *Nature*, 1991, **353**, 737-740.
2. A. Yella, H. W. Lee, H. N. Tsao, C. Y. Yi, A. K. Chandiran, M. K. Nazeeruddin, E. W. G. Diau, C. Y. Yeh, S. M. Zakeeruddin and M. Gratzel, *Science*, 2011, **334**, 629-634.
3. A. Hagfeldt, G. Boschloo, L. Sun, L. Kloo and H. Pettersson, *Chem. Rev*, 2010, **110**, 6595-6663.
4. Q. Zhang, C. S. Dandeneau, X. Zhou and G. Cao, *Adv. Mater*, 2009, **21**, 4087-4108.
5. Q. Zhang, T. R. Chou, B. Russo, S. A. Jenekhe and G. Cao, *Angew. Chem. Int. Ed.*, 2008, **47**, 2402-2406.
6. N. Memarian, I. Concina, A. Braga, S. M. Rozati, A. Vomiero and G. Sberveglieri, *Angew. Chem. Int. Ed.*, 2011, **50**, 12321-12325.
7. Y. Shi, C. Zhu, L. Wang, C. Zhao, W. Li, K. K. Fung, T. Ma, A. Hagfeldt and N. Wang, *Chem. Mater.*, 2013, **25**, 1000-1012.
8. Y. Shi, C. Zhu, L. Wang, W. Li, C. Cheng, K. M. Ho, K. K. Fung and N. Wang, *J. Mater. Chem.*, 2012, **22**, 13097-13103.
9. C. Cheng, Y. Shi, C. Zhu, W. Li, L. Wang, K. K. Fung and N. Wang, *Phys. Chem. Chem. Phys.*, 2011, **13**, 10631-10634.
10. Y. Shi, K. Wang, Y. Du, H. Zhang, J. Gu, C. Zhu, L. Wang, W. Guo, A. Hagfeldt, N. Wang and T. Ma, *Adv. Mater*, 2013, 10.1002/adma.201301852.
11. S. Ito, N.-L. C. Ha, G. Rothenberger, P. Liska, P. Comte, S. M. Zakeeruddin, P. Pechy, M. K. Nazeeruddin and M. Graetzel, *Chem. Commun*, 2006, 4004-4006.
12. X. Liu, Y. Luo, H. Li, Y. Fan, Z. Yu, Y. Lin, L. Chen and Q. Meng, *Chem. Commun*, 2007, 2847-2849.
13. Y.-H. Lai, C.-Y. Lin, H.-W. Chen, J.-G. Chen, C.-W. Kung, R. Vittal and K.-C. Ho, *J. Mater. Chem.*, 2010, **20**, 9379-9385.
14. L.-Y. Lin, M.-H. Yeh, C.-P. Lee, C.-Y. Chou, R. Vittal and K.-C. Ho, *Electrochim. Acta*, 2012, **62**, 341-347.
15. T. Guo, Y. Chen, L. Liu, Y. Cheng, X. Zhang, Q. Li, M. Wei and B. Ma, *J. Power Sources*, 2012, **201**, 408-412.
16. J.-Y. Liao, B.-X. Lei, H.-Y. Chen, D.-B. Kuang and C.-Y. Su, *Energy Environ. Sci.*, 2012, **5**, 5750-5757.
17. M. Ye, X. Xin, C. Lin and Z. Lin, *Nano Letters*, 2011, **11**, 3214-3220.
18. C. Xu, J. Wu, U. V. Desai and D. Gao, *J Am Chem Soc*, 2011, **133**, 8122-8125.
19. C. Y. Jiang, X. W. Sun, K. W. Tan, G. Q. Lo, A. K. K. Kyaw and D. L. Kwong, *Appl. Phys. Lett.*, 2008, **92**, 143101-143103.
20. W. Chen, Y. Qiu and S. Yang, *Phys. Chem. Chem. Phys.*, 2010, **12**, 9494-9501.
21. W. Chen, Y. Qiu and S. Yang, *Phys. Chem. Chem. Phys.*, 2012, **14**, 10872-10881.
22. Q. Zhang and G. Cao, *J. Mater. Chem.*, 2011, **21**, 6769.
23. S. Yodyingyong, Q. Zhang, K. Park, C. S. Dandeneau, X. Zhou, D. Triampo and G. Cao, *Appl. Phys. Lett.*, 2010, **96**, 073115.
24. L.-Y. Chen and Y.-T. Yin, *Nanoscale*, 2013, **5**, 1777-1780.
25. J. Tian, Q. Zhang, L. Zhang, R. Gao, L. Shen, S. Zhang, X. Qu and G. Cao, *Nanoscale*, 2013, **5**, 936-943.
26. H. Dong, L. Wang, R. Gao, B. Ma and Y. Qiu, *J. Mater. Chem.*, 2011, **21**, 19389-19394.
27. Y. Shi, C. Zhan, L. Wang, B. Ma, R. Gao, Y. Zhu and Y. Qiu, *Adv. Funct. Mater* 2010, **20**, 437-444.
28. R. Gao, Z. Liang, J. Tian, Q. Zhang, L. Wang and G. Cao, *Rsc. Adv*, 2013, **3**, 18537-18543.
29. R. Gao, Z. Liang, J. Tian, Q. Zhang, L. Wang and G. Cao, *Nano Energy*, 2013, **2**, 40-48.
30. R. Gao, L. Wang, Q. Zhang and G. Cao, *ECS Transactions*, 2013, **45**, 127-135.
31. X. F. Wu, H. Bai, C. Li, G. W. Lu and G. Q. Shi, *Chem. Commun*, 2006, 1655-1657.
32. R. Gao, J. Tian, Z. Liang, Q. Zhang, L. Wang and G. Cao, *Nanoscale*, 2013, **5**, 1894-1901.
33. J. B. Baxter and E. S. Aydil, *Sol. Energy Mater. Sol. Cells.*, 2006, **90**, 607-622.
34. S. Nakade, Y. Saito, W. Kubo, T. Kitamura, Y. Wada and S. Yanagida, *J. Phys. Chem. B*, 2003, **107**, 8607-8611.
35 M. J. Yang, B. Ding, S. Lee, J. K. Lee, *J. Phys. Chem. C*, 2011, **115**, 14534-14541.
36. W.-Q. Wu, H.-S. Rao, Y.-F. Xu, Y.-F. Wang, C.-Y. Su and D.-B. Kuang, *Sci. Rep*, 2013, **3**, 1892.

Graphical and textual abstract

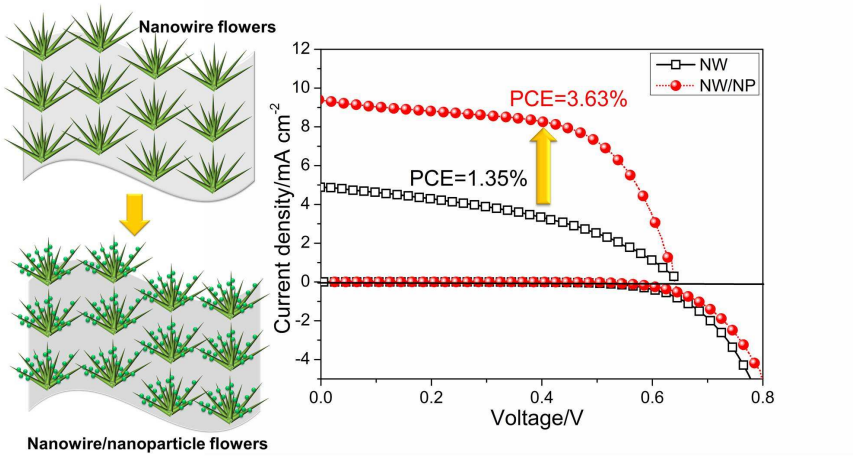

Nanorods/nanoparticels hierarchically structured ZnO were fabricated with a facile method as flexible photoanode with significant improved performance.